



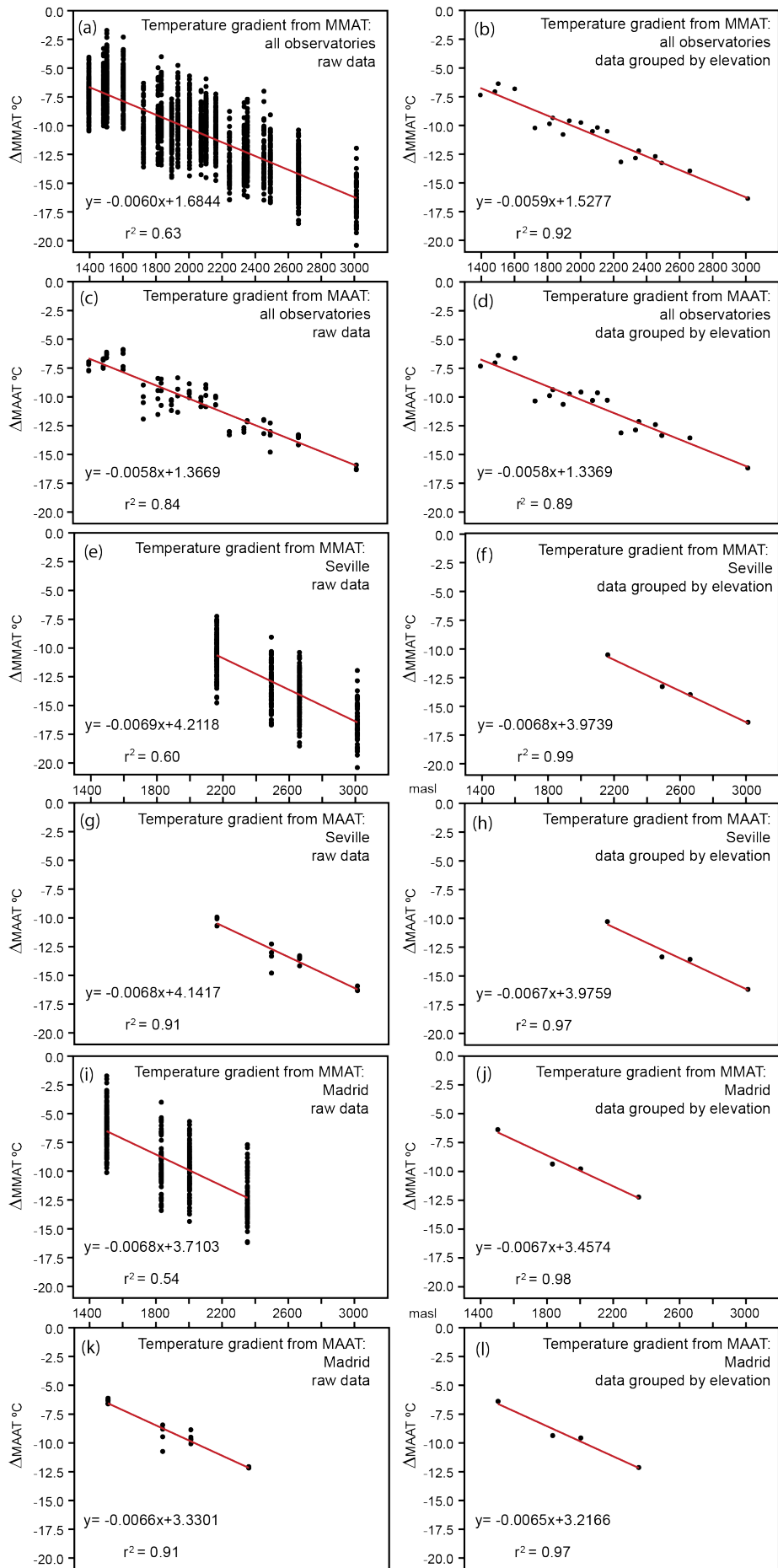
*Supplement of*

## **Algal lipids reveal unprecedented warming rates in alpine areas of SW Europe during the industrial period**

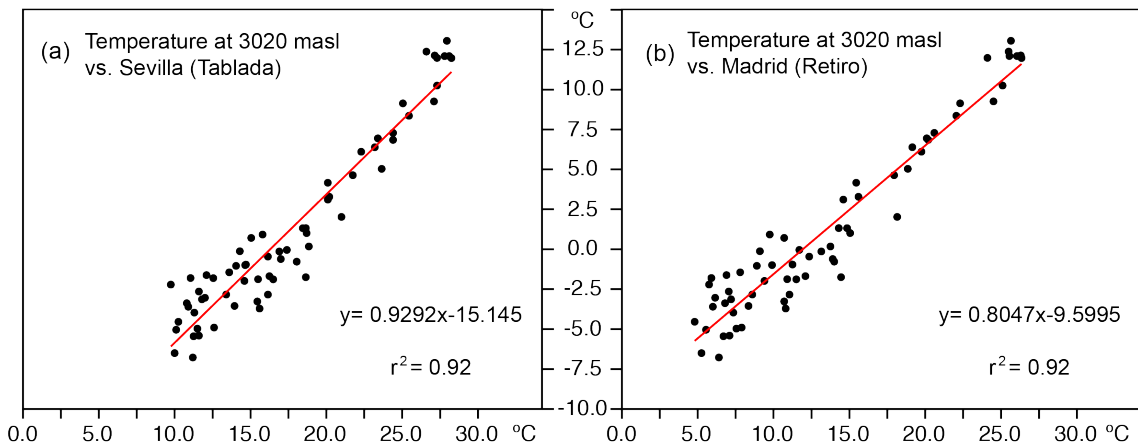
**Antonio García-Alix et al.**

*Correspondence to:* Antonio García-Alix (agalix@ugr.es)

The copyright of individual parts of the supplement might differ from the CC BY 4.0 License.

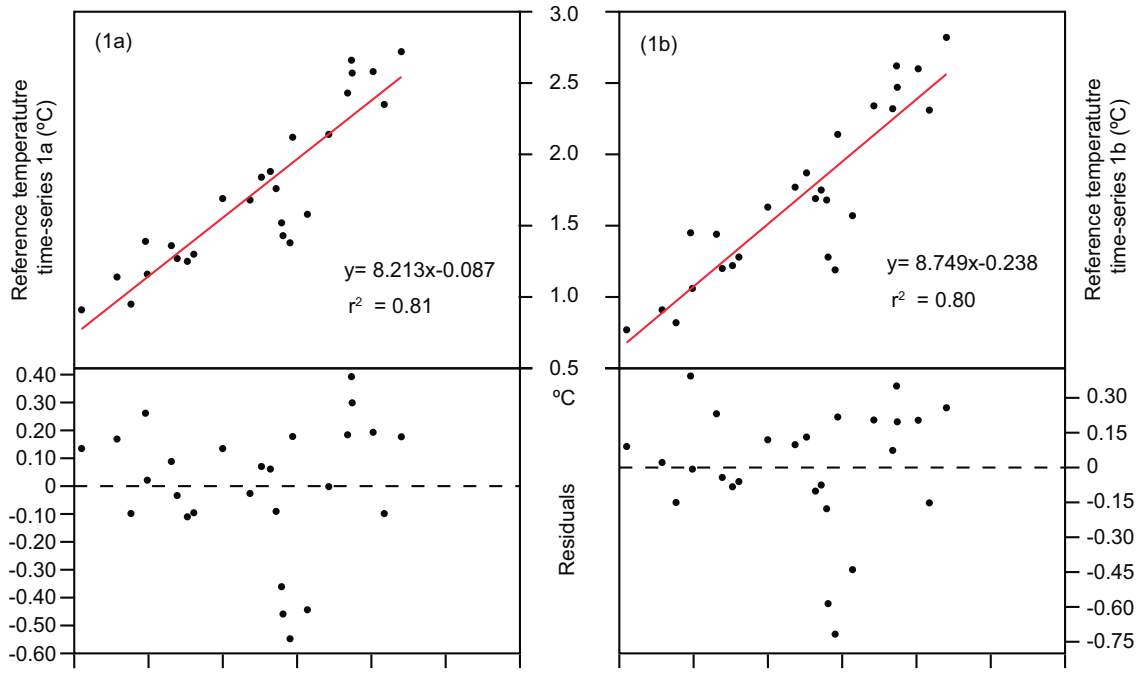


**Supplementary Figure S1.** Calculation of the Environmental Lapse Rate (ELR, °C/m) by means of ordinary least square regressions from temperature and elevation variations ( $\Delta_{\text{elevation}}$  and  $\Delta_{\text{MMAT}}$  or  $\Delta_{\text{MAAT}}$ ) between the low and high elevation observatories listed in Table S1 (data from Gonzalez-Hidalgo et al., 2015; Observatorio del cambio global de Sierra Nevada, 2019; Spanish National Weather Agency - AEMet Open Data, 2019; Staudt et al., 2007). MMAT (Monthly Mean Air Temperature) MAAT (Mean Annual Air Temperature). (a) raw  $\Delta_{\text{MMAT}}$  vs  $\Delta_{\text{elevation}}$  data (all observatories vs Sierra Nevada observatories); (b) mean  $\Delta_{\text{MMAT}}$  vs  $\Delta_{\text{elevation}}$  data grouped by elevation (all observatories vs Sierra Nevada observatories); (c) raw  $\Delta_{\text{MAAT}}$  vs  $\Delta_{\text{elevation}}$  data (all observatories vs Sierra Nevada observatories); (d) mean  $\Delta_{\text{MAAT}}$  vs  $\Delta_{\text{elevation}}$  data grouped by elevation (all observatories vs Sierra Nevada observatories); (e) raw  $\Delta_{\text{MMAT}}$  vs  $\Delta_{\text{elevation}}$  (Sevilla observatory vs Sierra Nevada observatories); (f) mean  $\Delta_{\text{MMAT}}$  vs  $\Delta_{\text{elevation}}$  (mean data grouped by elevation: Sevilla observatory vs Sierra Nevada observatories); (g) raw  $\Delta_{\text{MAAT}}$  vs  $\Delta_{\text{elevation}}$  (Sevilla observatory vs Sierra Nevada observatories); (h) mean  $\Delta_{\text{MAAT}}$  vs  $\Delta_{\text{elevation}}$  (mean data grouped by elevation: Sevilla observatory vs Sierra Nevada observatories); (i) raw  $\Delta_{\text{MMAT}}$  vs  $\Delta_{\text{elevation}}$  from (Madrid observatory vs Sierra Nevada observatories); (j) mean  $\Delta_{\text{MMAT}}$  vs  $\Delta_{\text{elevation}}$  (mean data grouped by elevation: Madrid observatory vs Sierra Nevada observatories); (k) raw  $\Delta_{\text{MAAT}}$  vs  $\Delta_{\text{elevation}}$  (Madrid observatory vs Sierra Nevada observatories); (l) mean  $\Delta_{\text{MAAT}}$  vs  $\Delta_{\text{elevation}}$  (mean data grouped by elevation: Madrid observatory vs Sierra Nevada observatories). The obtained ERLs (ranging from 0.0058°C/m to 0.0069°C/m) are certainly close to the global mean ERL (~0.0065°C/m) (International Civil Aviation Organization, 1993), showing that the different calculations are in agreement with the global temperature-elevation gradients.

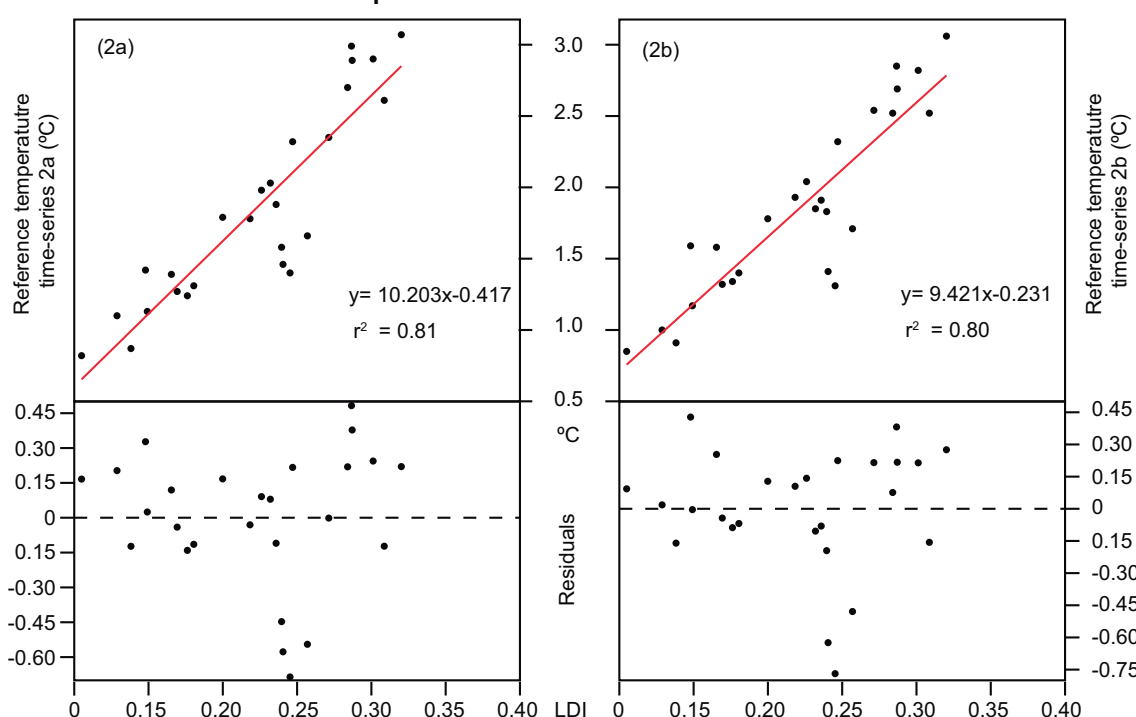


**Supplementary Figure S2.** (a) Correlation by means of ordinary least square regression between Sevilla monthly air temperatures and those from Cetursa 5 observatory (3020 masl). (b) Correlations by means of ordinary least square regression between Madrid monthly air temperatures and those from Cetursa 5 observatory (3020 masl) (data from Gonzalez-Hidalgo et al., 2015; Observatorio del cambio global de Sierra Nevada, 2019; Spanish National Weather Agency - AEMet Open Data, 2019; Staudt et al., 2007).

### LDI vs. reference temperature time-series 1 at 3020 masl from 1908 to 2008



### LDI vs. reference temperature time-series 2 at 3020 masl from 1908 to 2008



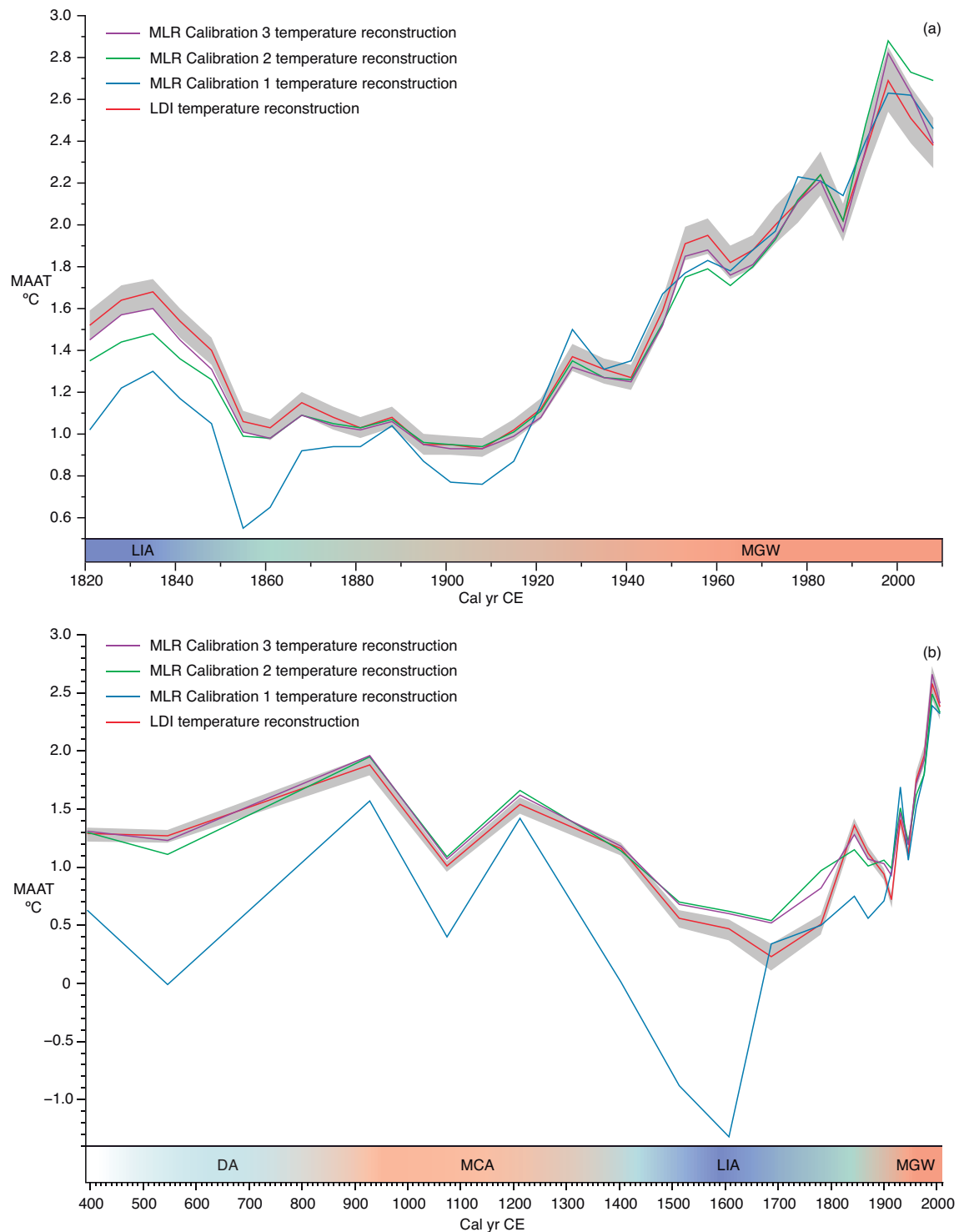
**Supplementary Figure S3.** LDI-temperature calibraton (ordinary least square regression) for each of the reference temperture time-series at 3020 masl from 1908 to 2008.

LDI calibration 1a: MAAT =  $8.213 \times \text{LDI} - 0.087$   $r^2=0.81$

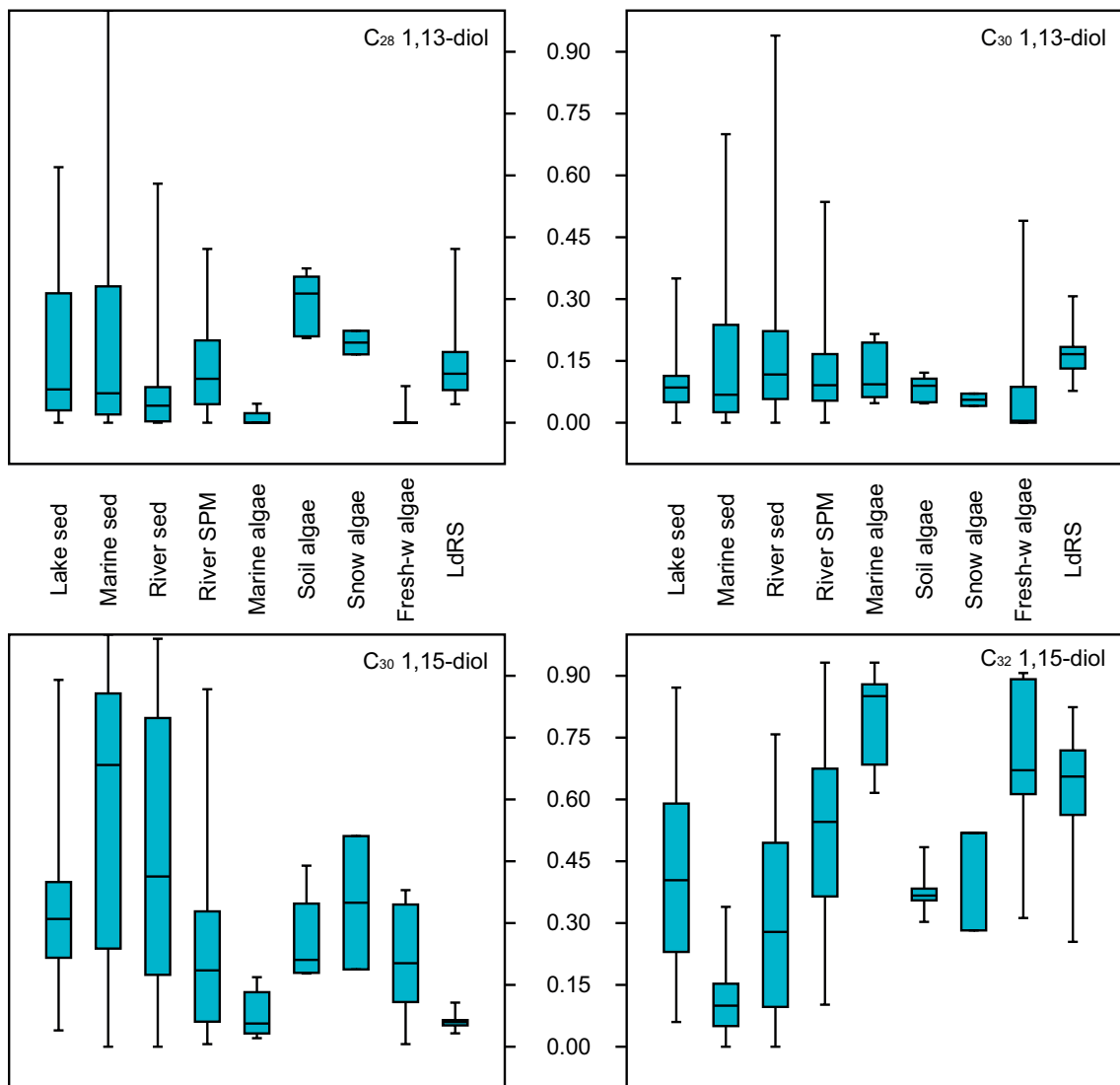
LDI calibration 1b: MAAT =  $8.749 \times \text{LDI} - 0.238$   $r^2=0.80$

LDI calibration 2a: MAAT =  $10.203 \times \text{LDI} - 0.417$   $r^2=0.81$

LDI calibration 2b: MAAT =  $9.421 \times \text{LDI} - 0.231$   $r^2=0.80$



**Supplementary Figure S4.** Comparison between the reconstructed mean annual air temperatures (MAAT) from both short and long LdRS records obtained from the different LCD-based temperature calibrations: 1) the LDI temperature calibration (Eq. 2: Fig. 3) along with its maximum and minimum range of variation from individual LDI-calibrations (grey shade), and 2) the MLR calibrations 1, 2 and 3 (Table S8). (a) Short core data (last ~200 years). (b) Long core data (last ~1500 years).



**Supplementary Figure S5.** Comparison by means of box-plot diagrams of the distribution of the relative abundances of the main LCDs from different sources and those from LdRS. Literature data from lake sediments (Rampen et al., 2014a), algal cultures (Rampen et al., 2014a), marine sediments (de Bar et al., 2016; Lattaud et al., 2017a; Rampen et al., 2014b; Rampen et al., 2012), river sediments/inputs (de Bar et al., 2016; Lattaud et al., 2017b), river particulate organic matter (Lattaud et al., 2018).

Observatory	Observatory elevation (masl)	Sierra Nevada (SN) observatory	SN Observatory elevation (masl)	$\Delta$ elevation (masl)
Sevilla (Tablada)	8	Albergue	2500	2492
Sevilla (Tablada)	8	Cetursa 1	2170	2162
Sevilla (Tablada)	8	Cetursa 3	2670	2662
Sevilla (Tablada)	8	Cetursa 5	3020	3012
Granada Airport	567	Albergue	2500	1933
Granada Airport	567	Cetursa 1	2170	1603
Granada Airport	567	Cetursa 3	2670	2103
Granada Airport	567	Cetursa 5	3020	2453
Madrid (Retiro)	667	Albergue	2500	1733
Madrid (Retiro)	667	Cetursa 1	2170	1503
Madrid (Retiro)	667	Cetursa 3	2670	2003
Madrid (Retiro)	667	Cetursa 5	3020	2353
Granada Armilla	687	Albergue	2500	1813
Granada Armilla	687	Cetursa 1	2170	1483
Granada Armilla	687	Cetursa 3	2670	1983
Granada Armilla	687	Cetursa 5	3020	2333
Granada Cartuja	775	Albergue	2500	1725
Granada Cartuja	775	Cetursa 1	2170	1395
Granada Cartuja	775	Cetursa 3	2670	1895
Granada Cartuja	775	Cetursa 5	3020	2245

**Supplementary Table S1.** Elevational difference between low and high elevation observatories used in this study. Observatories: Granada city (~30km from LdRS), Madrid (~360km from LdRS) and Sevilla (~230km from LdRS but almost similar latitude as LdRS).

Low vs high elevation observatories	Cetursa 5 3020 masl (n=67)		Cetursa 3 2670 masl (n=113)		Cetursa 1 2170 masl (n=121)		Albergue 2500 masl (n=72)	
	r	p	r	p	r	p	r	p
<b>Madrid 667 masl</b>	0.95920	7.99E-37	0.9671	8.28E-68	0.9641	2.44E-70	0.9598	2.40E-40
<b>Sevilla 8 masl</b>	0.95790	2.14E-36	0.9635	2.24E-65	0.9620	5.85E-69	0.9641	4.86E-42
<b>Gr-Airport 567 masl</b>	0.95430	2.80E-35	0.9655	4.18E-66	0.9626	8.66E-69	0.9591	4.37E-40
<b>Gr-Cartuja 775 masl</b>	0.96887	1.61E-40	0.9769	3.39E-76	0.9751	1.04E-79	0.9680	9.63E-44
<b>Gr-Armilla 687 masl</b>	0.96821	3.11E-40	0.9783	9.84E-78	0.9767	2.01E-81	0.9645	3.22E-42

**Supplementary Table S2.** Pearson correlations between mean monthly air temperatures (MMAT) from low and high elevation (Sierra Nevada) observatories (data from Gonzalez-Hidalgo et al., 2015; Observatorio del cambio global de Sierra Nevada, 2019; Spanish National Weather Agency - AEMet Open Data, 2019; Staudt et al., 2007). The Mann-Kendall test performed using PAST software (Hammer et al., 2001) in the raw data of these variables showed a  $p>0.05$  pointing towards no linear trends; therefore, no transformation has been applied.

LDI LdRS shc vs Low elevation observatories	n	LDI		C <sub>28</sub> 1,13-diol		C <sub>30</sub> 1,15-diol		C <sub>30</sub> 1,13-diol		C <sub>32</sub> 1,15-diol	
		r	p	r	p	r	p	r	p	r	p
Sevilla MAAT	19	0.91	6.6E-08	-0.86	2.4E-06	0.41	0.081	-0.91	6.0E-08	0.89	4.1E-07
Sevilla MWAT	19	0.72	5.6E-04	-0.70	9.5E-04	0.09	0.718	-0.75	2.3E-04	0.74	3.2E-04
Madrid MAAT	19	0.91	8.2E-08	-0.87	1.6E-06	0.34	0.155	-0.92	2.6E-08	0.90	1.5E-07
Madrid MWAT	19	0.77	1.3E-04	-0.76	1.4E-04	0.15	0.541	-0.82	1.8E-05	0.81	2.9E-05
Gr-Airport MAAT	19	0.71	7.2E-04	-0.62	5.0E-03	0.32	0.184	-0.72	5.1E-04	0.65	2.3E-03
Gr-Airport MWAT	19	0.58	9.5E-03	-0.56	1.3E-02	0.07	0.772	-0.63	4.0E-03	0.60	7.1E-03
Gr-Cartuja MAAT	19	0.73	3.7E-04	-0.70	9.2E-04	0.29	0.222	-0.76	1.5E-04	0.73	4.4E-04
Gr-Cartuja MWAT	19	0.65	2.8E-03	-0.65	2.8E-03	0.13	0.600	-0.70	8.6E-04	0.68	1.4E-03
Gr-Armilla MAAT	19	0.70	9.1E-04	-0.68	1.3E-03	0.31	0.203	-0.73	3.6E-04	0.70	7.5E-04
Gr-Armilla MWAT	19	0.61	5.6E-03	-0.64	2.9E-03	0.18	0.456	-0.66	2.0E-03	0.66	2.3E-03
LDI LdRS shc +lgc vs Low elevation observatories	n	LDI	C <sub>28</sub> 1,13-diol	C <sub>30</sub> 1,15-diol	C <sub>30</sub> 1,13-diol	C <sub>32</sub> 1,15-diol					
		r	p	r	p	r	p	r	p	r	p
Sevilla MAAT	26	0.89	7.5E-10	-0.72	3.9E-05	0.34	0.0855	-0.86	1.4E-08	0.79	1.8E-06
Sevilla MWAT	26	0.77	4.7E-06	-0.65	2.9E-04	0.20	0.3360	-0.74	1.5E-05	0.71	4.3E-05
Madrid MAAT	26	0.90	2.9E-10	-0.73	2.3E-05	0.30	0.1335	-0.88	2.7E-09	0.81	5.7E-07
Madrid MWAT	26	0.80	1.0E-06	-0.68	1.3E-04	0.22	0.2886	-0.79	1.5E-06	0.75	1.1E-05
Gr-Airport MAAT	26	0.69	9.5E-05	-0.55	3.4E-03	0.27	0.1748	-0.67	2.0E-04	0.61	1.0E-03
Gr-Airport MWAT	26	0.62	6.8E-04	-0.54	4.1E-03	0.19	0.3636	-0.61	1.1E-03	0.59	1.6E-03
Gr-Cartuja MAAT	26	0.74	1.4E-05	-0.65	3.5E-04	0.26	0.2075	-0.74	1.8E-05	0.70	6.8E-05
Gr-Cartuja MWAT	26	0.71	4.5E-05	-0.67	2.1E-04	0.23	0.2685	-0.69	8.5E-05	0.70	7.1E-05
Gr-Armilla MAAT	26	0.69	1.1E-04	-0.59	1.6E-03	0.25	0.2102	-0.68	1.2E-04	0.64	4.4E-04
Gr-Armilla MWAT	26	0.65	3.0E-04	-0.60	1.2E-03	0.24	0.2380	-0.64	4.8E-04	0.63	5.6E-04

**Supplementary Table S3.** Pearson correlations for the last ~100 years between LDI data in LdRS and temperature time-series of different observatories. Upper part: LDI LdRS shc data; lower part: LDI LdRS shc+lgc data. Mean annual air temperature (MAAT) and mean seasonal air temperatures from the warmer months (May-September: MWAT) have been tested (data from Gonzalez-Hidalgo et al., 2015; Spanish National Weather Agency - AEMet Open Data, 2019; Staudt et al., 2007). Although the reconstructed temperatures from Granada for the last ~100 years show a good correlation with the LCD distributions, they are likely biased by the low quality of the reconstructed data, since there are only reliable data from the 1970s onwards. In addition to the quality of the records (presence of gaps), this discrepancy between the LCD distribution in LdRS and Granada time-series could be linked to the strong control of Granada basin geomorphology in local rain and temperature patterns at low elevations, with local clouds and specific microclimate. Madrid and Sevilla area would not be influenced by those effects (Dogniaux, 1994).

LDI LdRS shc vs Low elevation observatories	n	Normal correlation		(z-score) <sup>2</sup> correlation		Mann- Kendall	Detrended correlation	
		r	p	r	p	no trend <i>p</i> >0.05	r	p
Sevilla MAAT	19	0.91	7E-08	0.89	2E-07	0.63	0.95	9E-10
Sevilla MWAT	19	0.72	0.0005	0.27	0.2719	0.04	0.40	0.0935
Madrid MAAT	19	0.91	8E-08	0.84	7E-06	0.65	0.93	9E-09
Madrid MWAT	19	0.77	0.0001	0.51	0.0267	0.09	0.64	0.0040
LDI LdRS shc+lgc vs Low elevation observatories	n	Normal correlation		(z-score) <sup>2</sup> correlation		Mann- Kendall	Detrended correlation	
		r	p	r	p	no trend <i>p</i> >0.05	r	p
Sevilla MAAT	26	0.89	8E-10	0.81	6E-07	0.57	0.86	1E-08
Sevilla MWAT	26	0.77	5E-06	0.44	0.02	0.03	0.57	0.002
Madrid MAAT	26	0.90	3E-10	0.76	6E-06	0.45	0.86	2E-08
Madrid MWAT	26	0.80	1E-06	0.56	0.003	0.06	0.68	0.0001

**Supplementary Table S4.** Pearson correlations (normal and detrended) for the last ~100 years between LDI data in LdRS and temperature time-series of different observatories. Upper part: LDI LdRS shc data; lower part: LDI LdRS shc+lgc data. Normal correlations show the relationship between long-term trends (data from Gonzalez-Hidalgo et al., 2015; Spanish National Weather Agency - AEMet Open Data, 2019; Staudt et al., 2007). Data were standardised (z-scores), normalised (squares) and a Mann-Kendall trend test was performed using PAST software (Hammer et al., 2001) in order to assess the existence of any trend over time in the data series. Afterwards, data were detrended by fitting a linear regression versus time, and a Pearson correlation was calculated with the residuals.

$\Delta_{\text{temperature}}$ vs $\Delta_{\text{elevation}}$	$\Delta_{\text{temp}}$ from <i>eq b</i> (global $\Delta_{\text{MMAT}}$ )	$\Delta_{\text{temp}}$ from <i>eq d</i> (global $\Delta_{\text{MAAT}}$ )	$\Delta_{\text{temp}}$ from <i>eqs f</i> and <i>j</i> (MMAT)	$\Delta_{\text{temp}}$ from <i>eqs h</i> and <i>l</i> (MAAT)	Real $\Delta_{\text{temp}}$ from MMAT	Real $\Delta_{\text{temp}}$ from MAAT
<b>Sevilla</b> <b>8 masl</b>	16.24 °C	16.13 °C	16.51 °C	16.20 °C	16.39 °C	16.17 °C
<b>Madrid</b> <b>667 masl</b>	12.36 °C	12.31 °C	12.31 °C	12.08 °C	12.23 °C	12.14 °C

**Supplementary Table S5.**  $\Delta_{\text{temperature}}$  between Madrid and Sevilla observatories and Cetursa5 (at the same elevation as LdRS, 3020 masl) calculated using different approaches: 1) using equation from Fig. S1b from the mean values between  $\Delta_{\text{MMAT}}$  and  $\Delta_{\text{elev}}$  among all the studied low elevation observatories vs those from high elevation areas; 2) the same as the previous one but with the  $\Delta_{\text{MAAT}}$  (equation from Fig. S1d); 3) using equations from Fig. S1f and j (Sevilla-Madrid respectively) from the mean values between  $\Delta_{\text{MMAT}}$  and  $\Delta_{\text{elev}}$  of Sevilla or Madrid observatories respectively vs those from high elevation areas; 4) the same as the previous one but with the  $\Delta_{\text{MAAT}}$  (equations from Fig. S1h and l); 5) real  $\Delta_{\text{MMAT}}$  between Sevilla or Madrid observatories and Cetursa 5 observatory (3020 masl); 6) the same as the previous one but with the  $\Delta_{\text{MAAT}}$ .

<b>LdRS shc n=32</b>	<b>C<sub>28</sub> 1,13-diol</b>	<b>C<sub>30</sub> 1,15-diol</b>	<b>C<sub>30</sub> 1,13-diol</b>	<b>C<sub>32</sub> 1,15-diol</b>
<b>C<sub>28</sub> 1,13-diol</b>		4.8E-06	1.8E-07	9.4E-14
<b>C<sub>30</sub> 1,15-diol</b>	-0.71		0.005	0.001
<b>C<sub>30</sub> 1,13-diol</b>	0.78	-0.49		1.2E-17
<b>C<sub>32</sub> 1,15-diol</b>	-0.92	0.57	-0.96	
<b>LdRS lgc n=20</b>	<b>C<sub>28</sub> 1,13-diol</b>	<b>C<sub>30</sub> 1,15-diol</b>	<b>C<sub>30</sub> 1,13-diol</b>	<b>C<sub>32</sub> 1,15-diol</b>
<b>C<sub>28</sub> 1,13-diol</b>		0.02	1.2E-09	9.2E-14
<b>C<sub>30</sub> 1,15-diol</b>	-0.53		0.07	0.07
<b>C<sub>30</sub> 1,13-diol</b>	0.94	-0.42		5.5E-14
<b>C<sub>32</sub> 1,15-diol</b>	-0.98	0.42	-0.98	

**Supplementary Table S6.** Pearson correlation table ( $r$  vs  $p$ ) for the relative abundances of the dominant LCDs in both short and long LdRS cores (shc and lgc).

LCDs vs reference MAAT at 3020 masl	LdRS shc		LdRS she+lgc	
	r	p	r	p
<b>LDI</b>	0.90	2E-28	0.90	2E-36
<b>C<sub>28</sub> 1,13-diol</b>	-0.85	2E-22	-0.72	1E-17
<b>C<sub>30</sub> 1,15-diol</b>	0.37	9E-04	0.32	9E-04
<b>C<sub>30</sub> 1,13-diol</b>	-0.90	4E-29	-0.86	4E-32
<b>C<sub>32</sub> 1,15-diol</b>	0.89	2E-27	0.79	2E-23

**Supplementary Table S7.** Pearson correlations between the relative abundances of the dominant LCDs in both short and long LdRS cores (shc and lgc), the LDI values, and the mean reconstructed reference temperature time-series at 3020 masl for the last ~100 years.

Calibrations	Variable	r	p	$r^2$
<b>Calibration 1:</b> Fractional abundances of LCDs:	C <sub>28</sub> 1,13-diol	-0.72	1E-17	0.51
	C <sub>30</sub> 1,15-diol	0.32	9E-04	0.10
	C <sub>30</sub> 1,13-diol	-0.86	4E-32	0.75
	C <sub>32</sub> 1,15-diol	0.79	2E-23	0.62
<b>Calibration 2 and 3:</b> Ratio of fractional abundances of LCDs:	C <sub>30</sub> 1,15- / C <sub>28</sub> 1,13-diols	0.87	8E-34	0.76
	C <sub>30</sub> 1,15- / C <sub>30</sub> 1,13-diols	0.89	6E-37	0.80
	C <sub>32</sub> 1,15- / C <sub>28</sub> 1,13-diols	0.85	1E-29	0.72
	C <sub>32</sub> 1,15- / C <sub>30</sub> 1,13-diols	0.87	3E-33	0.76

**Supplementary Table S8.** Comparison between the different statistics of the potential LCD-based temperature calibrations computed by means of multiple linear regressions and the reference temperature time-series at 3020 masl for the last ~100 years. The obtained calibration equations are:

- MLR Calibration 1:

$$\text{MAAT} = 3.16 - 0.48 * \text{RA}_{\text{C}28\ 1,13-\text{diol}} + 12.87 * \text{RA}_{\text{C}30\ 1,15-\text{diol}} - 16.43 * \text{RA}_{\text{C}30\ 1,13-\text{diol}}$$

$$r^2=0.78$$

- MLR Calibration 2:

$$\text{MAAT} = 0.005 - 1.14 * \text{RA}_{(\text{C}30\ 1,15- / \text{C}28\ 1,13-\text{diols})} + 4.21 * \text{RA}_{(\text{C}30\ 1,15- / \text{C}30\ 1,13-\text{diols})} + 0.14 * \text{RA}_{(\text{C}32\ 1,15- / \text{C}28\ 1,13-\text{diols})} - 0.12 * \text{RA}_{(\text{C}32\ 1,15- / \text{C}30\ 1,13-\text{diols})}$$

$$r^2=0.83$$

- MLR Calibration 3:

$$\text{MAAT} = 0.03 + 0.74 * \text{RA}_{(\text{C}30\ 1,15- / \text{C}28\ 1,13-\text{diols})} + 2.44 * \text{RA}_{(\text{C}30\ 1,15- / \text{C}30\ 1,13-\text{diols})}$$

$$r^2=0.81$$

LdRS vs	Lake sed	Marine sed	River sed	River SPM	Marine algae	Soil algae	Snow algae	Fresh-w algae
C <sub>28</sub> 1,13-diol	ns	ns	***	ns	***	**	ns	***
C <sub>30</sub> 1,13-diol	***	**	*	***	ns	**	**	**
C <sub>30</sub> 1,15-diol	***	***	***	***	ns	***	**	**
C <sub>32</sub> 1,15-diol	***	***	***	***	*	**	§	ns

**Supplementary Table S9.** Results of the Mann-Whitney U test that has been performed to identify the differences between individual isomers from LdRS and those from other sources. Literature data from: lake sediments (Rampen et al., 2014a), algal cultures (Rampen et al., 2014a), marine sediments (de Bar et al., 2016; Lattaud et al., 2017a; Rampen et al., 2014b; Rampen et al., 2012), river sediments/inputs (de Bar et al., 2016; Lattaud et al., 2017b), river particulate organic matter (Lattaud et al., 2018). Significant level for the differences between LdRS and other source groups: \*\*\*  $p < 0.001$ ; \*\*  $0.001 < p < 0.01$ ; \*  $0.01 < p < 0.05$ ; §  $0.05 < p < 0.1$ ; ns  $p > 0.1$ .

LdRS shc LDI vs		n	Normal correlation		(z-score) <sup>2</sup> correlation		Mann-Kendall	Detrended correlation	
			r	p	r	p	no trend p>0.05	r	p
Solar	ΔTSI	32	0.58	0.0004	-0.10	0.5891	0.96	-0.03	0.8893
	TSI	32	0.56	0.0009	0.10	0.5675	0.87	0.02	0.9120
Volcanic	NH volcanic aerosol	27	0.15	0.4201	0.09	0.6435	0.66	0.03	0.8677
	Global volcanic aerosol	27	0.19	0.3235	-0.002	0.9926	0.93	0.06	0.7584
	*Global volcanic forcing	27	-0.04	0.8442	0.04	0.8392	0.59	0.12	0.5181
Atmospheric	NAO	30	-0.03	0.8830	0.33	0.0772	3E-05	0.05	0.7760
	AMO	32	0.61	0.0002	0.41	0.0210	0.37	0.32	0.0711
Green house gases	CO <sub>2</sub> (ppm)	31	0.83	6E-09	0.77	5E-07	0.36	0.70	0.0000
	NO <sub>2</sub> (ppm)	31	0.85	1E-09	0.78	2E-07	0.46	0.71	0.0000
	CH <sub>4</sub> (ppm)	31	0.86	5E-10	0.73	2E-06	0.56	0.65	0.0001
Temperatures	CPS Summer temperatures	32	0.58	0.0007	0.44	0.0131	0.30	0.40	0.0261
	U <sup>K</sup> <sub>37</sub> -SST Gol-Ho1B	32	0.76	4E-07	0.24	0.1884	0.83	0.16	0.3739
	Global Temperatures (GLSS)	19	0.89	3E-07	0.69	0.0010	0.62	0.74	0.0003

**Supplementary Table S10.** Pearson correlations (normal and detrended) between the LDI record from the LdRS short core and different proxies for solar and volcanic forcing, North Atlantic modes, greenhouse gases, and temperatures. Normal correlations show long-term trends. Data were standardised (z-scores), normalised (squares) and a Mann-Kendall trend test was performed using PAST software (Hammer et al., 2001) in order to assess the existence of any trend over time in the data series. Afterwards, data were detrended by fitting a linear regression versus time, and a Pearson correlation was worked out with the residuals. \*: Note that inverse global volcanic forcing values have been used in order to show the same trends as in Fig. 5.

**Solar Proxies:** ΔTSI, reconstruction of the difference of the total solar irradiance from the value of the PMOD composite series during the solar cycle minimum of the year 1986 CE ( $1365.57 \text{ W m}^{-2}$ ) (Steinhilber et al., 2009); TSI, total solar Irradiance (Coddington et al., 2016).

**Volcanic proxies:** Annual stratospheric volcanic sulfate aerosol injection for the past 1500 years in the North Hemisphere and worldwide (Gao et al., 2008); global volcanic aerosol forcing ( $\text{W m}^{-2}$ ) (Sigl et al., 2015).

**North Atlantic modes:** NAO, North Atlantic Oscillation reconstruction (Trouet et al., 2009); AMO, Atlantic Multidecadal Oscillation reconstruction (Mann et al., 2009).

**Greenhouse gases:** Reconstructed concentrations of atmospheric CO<sub>2</sub>, NO<sub>2</sub>, and CH<sub>4</sub> (ppm) (Schmidt et al., 2011).

**Temperatures:** Composite-plus-scaling (CPS) mean summer temperature anomaly reconstruction from tree rings records in Europe with respect to 1974-2003 CE (MSTA °C) (Luterbacher et al., 2016); U<sup>K</sup><sub>37</sub>-derived SSTs from the marine record in the Gulf of Lion (NW Mediterranean Sea) (Sicre et al., 2016), and global land and sea surface (GLSS) mean annual temperature anomalies with respect to 1979-2008 CE (Hansen et al., 2010).

LdRS lgc LDI vs		n	Normal correlation		(z-score) <sup>2</sup> correlation		Mann-Kendall	Detrended correlation	
			r	p	r	p	no trend p>0.05	r	p
Solar	* $\Delta^{14}\text{C}$	16	-0.73	0.0015	0.40	0.1301	0.19	0.38	0.1454
	$\Delta\text{TSI}$	20	0.69	0.0007	0.38	0.1024	0.02	0.367	0.1117
	TSI	13	0.88	0.0001	0.13	0.0863	0.85	0.56	0.0451
Volcanic	NH volcanic aerosol	19	-0.07	0.7758	0.13	0.5932	0.16	0.13	0.5932
	Global volcanic aerosol	19	0.06	0.7922	0.28	0.2517	0.05	0.28	0.2517
	*Global volcanic forcing	16	-0.03	0.8948	0.32	0.1564	0.07	0.33	0.1564
North Atlantic modes	NAO	16	0.10	0.7127	0.33	0.2098	0.30	0.23	0.3890
	AMO	19	0.60	0.0064	0.37	0.1156	0.48	0.25	0.2928
Greenhouse gases	CO <sub>2</sub> (ppm)	20	0.74	0.0002	0.73	0.0003	0.97	0.65	0.0018
	NO <sub>2</sub> (ppm)	20	0.65	0.0018	0.68	0.0009	0.92	0.61	0.0043
	CH <sub>4</sub> (ppm)	20	0.73	0.0003	0.77	0.0001	0.35	0.71	0.0005
Temperatures	CPS Summer temperatures	20	0.71	0.0005	0.46	0.0420	0.18	0.34	0.1421
	U <sup>K</sup> <sub>37</sub> -SST Gol-Ho1B	20	0.61	0.0043	0.72	0.0003	0.12	0.65	0.0018
	U <sup>K</sup> <sub>37</sub> -SST TTR-17-384B	17	0.24	0.3581	0.02	0.9374	0.77	0.01	0.9537
	TEX <sup>H</sup> <sub>86</sub> -SST TTR-17-384B	17	0.45	0.0707	0.53	0.0299	0.97	0.47	0.0538
	U <sup>K</sup> <sub>37</sub> -SST TTR-17-436B	18	0.34	0.1697	0.68	0.0020	0.32	0.70	0.0013
	TEX <sup>H</sup> <sub>86</sub> -SST TTR-17-436B	18	0.43	0.0721	0.18	0.4830	0.40	0.34	0.1610

**Supplementary Table S11.** Pearson correlations (normal and detrended) between the LDI record from the LdRS long core and different proxies for solar and volcanic forcing, North Atlantic modes, greenhouse gases, and temperatures. Normal correlations show long-term trends. Data were standardised (z-scores), normalised (squares), and a Mann-Kendall trend test was performed using PAST software (Hammer et al., 2001) in order to assess the existence of any trend over time in the data series. Afterwards, data were detrended by fitting a linear regression versus time, and a Pearson correlation was worked out with the residuals. \*: Note that inverse  $\Delta^{14}\text{C}$  and global volcanic forcing values have been used in order to show the same trends as in Fig. 6.

**Solar Proxies:**  $\Delta^{14}\text{C}$  (Reimer et al., 2013);  $\Delta\text{TSI}$ , reconstruction of the difference of the total solar irradiance from the value of the PMOD composite series during the solar cycle minimum of the year 1986 CE ( $1365.57 \text{ W m}^{-2}$ ) (Steinhilber et al., 2009); TSI, total solar irradiance (Coddington et al., 2016).

**Volcanic proxies:** Annual stratospheric volcanic sulfate aerosol injection for the past 1500 years in the North Hemisphere, and worldwide (Gao et al., 2008); global volcanic aerosol forcing ( $\text{W m}^{-2}$ ) (Sigl et al., 2015).

**North Atlantic modes:** NAO, North Atlantic Oscillation reconstruction (Trouet et al., 2009); AMO, Atlantic Multidecadal Oscillation reconstruction (Mann et al., 2009).

**Greenhouse gases:** Reconstructed concentrations of atmospheric CO<sub>2</sub>, NO<sub>2</sub>, and CH<sub>4</sub> (ppm) (Schmidt et al., 2011).

**Temperatures:** Composite-plus-scaling (CPS) mean summer temperature anomaly reconstruction from tree rings records in Europe with respect to 1974-2003 CE (MSTA °C); U<sup>K</sup><sub>37</sub>-derived SSTs from the marine record in the Gulf of Lion (NW Mediterranean Sea) (Sicre et al., 2016); U<sup>K</sup><sub>37</sub>-and TEX<sub>86</sub>-derived SSTs records from cores 384B and 436B in the Alboran Sea (Nieto-Moreno et al., 2013).

LdRS shc vs		n	MLR calibration 1		MLR calibration 2		MLR calibration 3	
			r	p	r	p	r	p
Solar	<b>ΔTSI</b>	32	0.69	1.3E-05	0.60	2.6E-04	0.59	4.1E-04
	<b>TSI</b>	32	0.63	1.1E-04	0.55	1.1E-03	0.55	1.0E-03
Volcanic	<b>NH volcanic aerosol</b>	27	0.13	0.4912	0.13	0.4843	0.14	0.4523
	<b>Global volcanic aerosol</b>	27	0.15	0.4232	0.17	0.3581	0.18	0.3438
	<b>*Global volcanic forcing</b>	27	0.04	0.8212	-0.01	0.9597	-0.02	0.9168
Atmospheric	<b>NAO</b>	30	0.01	0.9784	0.08	0.6620	0.03	0.8939
	<b>AMO</b>	32	0.71	4.3E-06	0.69	1.2E-05	0.63	9.8E-05
Green house gases	<b>CO<sub>2</sub> (ppm)</b>	31	0.92	2.5E-13	0.90	2.8E-12	0.86	4.6E-10
	<b>NO<sub>2</sub> (ppm)</b>	31	0.93	2.7E-14	0.92	2.6E-13	0.88	6.6E-11
	<b>CH<sub>4</sub> (ppm)</b>	31	0.94	4.9E-15	0.92	4.7E-13	0.88	6.3E-11
Temperatures	<b>CPS Summer temperatures</b>	32	0.66	5.2E-05	0.65	8.9E-05	0.61	2.9E-04
	<b>U<sup>K</sup><sub>37</sub>-SST Gol-Ho1B</b>	32	0.86	2.2E-10	0.80	2.9E-08	0.77	2.4E-07
	<b>Global Temperatures (GLSS)</b>	19	0.90	7.4E-09	0.93	1.0E-10	0.90	4.2E-09

**Supplementary Table S12.** Pearson correlations between the reconstructed temperatures in the LdRS shc from MLR calibrations 1, 2, and 3 and different proxies for solar and volcanic forcing, North Atlantic modes, greenhouse gases, and temperatures. Note that inverse global volcanic forcing values have been used in order to show the same trends as in Fig. 5. Proxy explanation as in Supplementary Table S10.

LdRS lgc vs		n	MLR calibration 1		MLR calibration 2		MLR calibration 3	
			r	p	r	p	r	p
Solar	* $\Delta^{14}\text{C}$	16	-0.57	0.0202	-0.73	0.0013	-0.73	0.0012
	$\Delta\text{TSI}$	20	0.71	0.0005	0.71	0.0004	0.71	0.0005
	TSI	13	0.84	0.0003	0.86	0.0001	0.86	0.0002
Volcanic	NH volcanic aerosol	19	0.09	0.7058	0.06	0.7959	0.01	0.9723
	Global volcanic aerosol	19	0.05	0.8245	0.16	0.5235	0.13	0.5925
	*Global volcanic forcing	16	0.05	0.8287	-0.08	0.7238	-0.08	0.7486
North Atlantic modes	NAO	16	-0.01	0.9746	0.15	0.5775	0.13	0.6378
	AMO	19	0.52	0.0225	0.63	0.0036	0.61	0.0054
Greenhouse gases	CO <sub>2</sub> (ppm)	20	0.74	0.0002	0.76	0.0001	0.77	0.0001
	NO <sub>2</sub> (ppm)	20	0.74	0.0002	0.68	0.0009	0.69	0.0009
	CH <sub>4</sub> (ppm)	20	0.73	0.0003	0.75	0.0002	0.76	0.0001
Temperatures	CPS Summer temperatures	20	0.72	0.0004	0.75	0.0001	0.73	0.0002
	U <sup>K</sup> <sub>37</sub> -SST Gol-Ho1B	20	0.63	0.0031	0.65	0.0020	0.65	0.0019
	U <sup>K</sup> <sub>37</sub> -SST TTR-17-384B	17	0.38	0.1342	0.20	0.4464	0.19	0.4703
	TEX <sup>H</sup> <sub>86</sub> -SST TTR-17-384B	17	0.20	0.4314	0.46	0.0605	0.47	0.0552
	U <sup>K</sup> <sub>37</sub> -SST TTR-17-436B	18	0.39	0.1103	0.41	0.0951	0.37	0.1274
	TEX <sup>H</sup> <sub>86</sub> -SST TTR-17-436B	18	0.30	0.2318	0.51	0.0305	0.47	0.0516

**Supplementary Table S13.** Pearson correlations between reconstructed temperatures in the LdRS lgc from calibrations 1, 2, and 3 and different proxies for solar and volcanic forcing, North Atlantic modes, greenhouse gases, and temperatures. Note that inverse  $\Delta^{14}\text{C}$  and global volcanic forcing values have been used in order to show the same trends as in Fig. 6. Proxy explanation as in Supplementary Table S11.

## Supplementary References

- Coddington, O., Lean, J. L., Pilewskie, P., Snow, M., and Lindholm, D.: A Solar Irradiance Climate Data Record, *Bulletin of the American Meteorological Society*, 97, 1265-1282, 2016.
- de Bar, M. W., Dorhout, D. J. C., Hopmans, E. C., Rampen, S. W., Sinninghe Damsté, J. S., and Schouten, S.: Constraints on the application of long chain diol proxies in the Iberian Atlantic margin, *Organic Geochemistry*, 101, 184-195, 2016.
- Dogniaux, R.: Prediction of Solar Radiation in Areas with a Specific Microclimate, *Prediction of Solar Radiation in Areas with a Specific Microclimate*, 1994.
- Gao, C., Robock, A., and Ammann, C.: Volcanic forcing of climate over the past 1500 years: An improved ice core-based index for climate models, *Journal of Geophysical Research: Atmospheres*, 113, 2008.
- Gonzalez-Hidalgo, J. C., Peña-Angulo, D., Brunetti, M., and Cortesi, N.: MOTEDAS: a new monthly temperature database for mainland Spain and the trend in temperature (1951–2010), *International Journal of Climatology*, 35, 4444-4463, 2015.
- Hammer, Ø., Harper, D. A. T., and Ryan, P. D.: PAST: Paleontological statistics software package for education and data analysis, *Palaeontologia Electronica* 4, 9, 2001.
- Hansen, J., Ruedy, R., Sato, M., and Lo, K.: Global Surface Temperature Change, *Reviews of Geophysics*, 48, 2010.
- International-Civil-Aviation-Organization: Manual of the ICAO standard atmosphere : extended to 80 kilometres (262 500 feet) (Third ed.), International Civil Aviation Organization, Montreal, Quebec, 1993.
- Lattaud, J., Dorhout, D., Schulz, H., Castañeda, I. S., Schefuß, E., Sinninghe Damsté, J. S., and Schouten, S.: The C32 alkane-1,15-diol as a proxy of late Quaternary riverine input in coastal margins, *Clim. Past*, 13, 1049-1061, 2017a.
- Lattaud, J., Kim, J.-H., De Jonge, C., Zell, C., Sinninghe Damsté, J. S., and Schouten, S.: The C32 alkane-1,15-diol as a tracer for riverine input in coastal seas, *Geochimica et Cosmochimica Acta*, 202, 146-158, 2017b.
- Lattaud, J., Kirkels, F., Peterse, F., Freymond, C. V., Eglinton, T. I., Heftet, J., Mollenhauer, G., Balzano, S., Villanueva, L., van der Meer, M. T. J., Hopmans, E. C., Sinninghe Damsté, J. S., and Schouten, S.: Long-chain diols in rivers: distribution and potential biological sources, *Biogeosciences*, 15, 4147-4161, 2018.
- Luterbacher, J., Werner, J. P., Smerdon, J. E., Fernández-Donado, L., González-Rouco, F. J., Barriopedro, D., Ljungqvist, F. C., Büntgen, U., Zorita, E., Wagner, S., Esper, J., McCarroll, D., Toreti, A., Frank, D., Jungclaus, J. H., Barriendos, M., Bertolin, C., Bothe, O., Brázdil, R., Camuffo, D., Dobrovolný, P., Gagen, M., García-Bustamante, E., Ge, Q., Gómez-Navarro, J. J., Guiot, J., Hao, Z., Hegerl, G. C., Holmgren, K., Klimenko, V. V., Martín-Chivelet, J., Pfister, C., Roberts, N., Schindler, A., Schurer, A., Solomina, O., von Gunten, L., Wahl, E., Wanner, H., Wetter, O., Xoplaki, E., Yuan, N., Zanchettin, D., Zhang, H., and Zerefos, C.: European summer temperatures since Roman times, *Environmental Research Letters*, 11, 024001, 2016.

- Mann, M. E., Zhang, Z., Rutherford, S., Bradley, R. S., Hughes, M. K., Shindell, D., Ammann, C., Faluvegi, G., and Ni, F.: Global Signatures and Dynamical Origins of the Little Ice Age and Medieval Climate Anomaly, *Science*, 326, 1256-1260, 2009.
- Nieto-Moreno, V., Martínez-Ruiz, F., Willmott, V., García-Orellana, J., Masqué, P., and Sinninghe Damsté, J. S.: Climate conditions in the westernmost Mediterranean over the last two millennia: An integrated biomarker approach, *Organic Geochemistry*, 55, 1-10, 2013.
- Observatorio del cambio global de Sierra Nevada: Linaria v1.0. iEcolab – Laboratorio de Ecología Terrestre – Universidad de Granada, <http://linaria.obsnev.es>, 2019.
- Rampen, S. W., Datema, M., Rodrigo-Gámiz, M., Schouten, S., Reichart, G.-J., and Sinninghe Damsté, J. S.: Sources and proxy potential of long chain alkyl diols in lacustrine environments, *Geochimica et Cosmochimica Acta*, 144, 59-71, 2014a.
- Rampen, S. W., Willmott, V., Kim, J.-H., Rodrigo-Gámiz, M., Uliana, E., Mollenhauer, G., Schefuß, E., Sinninghe Damsté, J. S., and Schouten, S.: Evaluation of long chain 1,14-alkyl diols in marine sediments as indicators for upwelling and temperature, *Organic Geochemistry*, 76, 39-47, 2014b.
- Rampen, S. W., Willmott, V., Kim, J.-H., Uliana, E., Mollenhauer, G., Schefuß, E., Sinninghe Damsté, J. S., and Schouten, S.: Long chain 1,13- and 1,15-diols as a potential proxy for palaeotemperature reconstruction, *Geochimica et Cosmochimica Acta*, 84, 204-216, 2012.
- Reimer, P. J., Bard, E., Bayliss, A., Beck, J. W., Blackwell, P. G., Ramsey, C. B., Buck, C. E., Cheng, H., Edwards, R. L., Friedrich, M., Grootes, P. M., Guilderson, T. P., Haflidason, H., Hajdas, I., Hatté, C., Heaton, T. J., Hoffmann, D. L., Hogg, A. G., Hughen, K. A., Kaiser, K. F., Kromer, B., Manning, S. W., Niu, M., Reimer, R. W., Richards, D. A., Scott, E. M., Sounthor, J. R., Staff, R. A., Turney, C. S. M., and van der Plicht, J.: IntCal13 and Marine13 Radiocarbon Age Calibration Curves 0–50,000 Years cal BP, *Radiocarbon*, 55, 1869-1887, 2013.
- Schmidt, G. A., Jungclaus, J. H., Ammann, C. M., Bard, E., Braconnot, P., Crowley, T. J., Delaygue, G., Joos, F., Krivova, N. A., Muscheler, R., Otto-Bliesner, B. L., Pongratz, J., Shindell, D. T., Solanki, S. K., Steinhilber, F., and Vieira, L. E. A.: Climate forcing reconstructions for use in PMIP simulations of the last millennium (v1.0), *Geosci. Model Dev.*, 4, 33-45, 2011.
- Sicre, M.-A., Jalali, B., Martrat, B., Schmidt, S., Bassetti, M.-A., and Kallel, N.: Sea surface temperature variability in the North Western Mediterranean Sea (Gulf of Lion) during the Common Era, *Earth and Planetary Science Letters*, 456, 124-133, 2016.
- Sigl, M., Winstrup, M., McConnell, J. R., Welten, K. C., Plunkett, G., Ludlow, F., Buntgen, U., Caffee, M., Chellman, N., Dahl-Jensen, D., Fischer, H., Kipfstuhl, S., Kostick, C., Maselli, O. J., Mekhaldi, F., Mulvaney, R., Muscheler, R., Pasteris, D. R., Pilcher, J. R., Salzer, M., Schupbach, S., Steffensen, J. P., Vinther, B. M., and Woodruff, T. E.: Timing and climate forcing of volcanic eruptions for the past 2,500 years, *Nature*, 523, 543-549, 2015.

- Spanish National Weather Agency - AEMet Open Data: AEMet Open Data.  
[http://www.aemet.es/es/datos\\_abiertos/AEMET\\_OpenData](http://www.aemet.es/es/datos_abiertos/AEMET_OpenData), 2019.
- Staudt, M., Esteban-Parra, M. J., and Castro-Díez, Y.: Homogenization of long-term monthly Spanish temperature data, *International Journal of Climatology*, 27, 1809-1823, 2007.
- Steinhilber, F., Beer, J., and Fröhlich, C.: Total solar irradiance during the Holocene, *Geophysical Research Letters*, 36, 2009.
- Trouet, V., Esper, J., Graham, N. E., Baker, A., Scourse, J. D., and Frank, D. C.: Persistent Positive North Atlantic Oscillation Mode Dominated the Medieval Climate Anomaly, *Science*, 324, 78-80, 2009.